*J Mater Sci* (2019) 54:11390–11399

Ceramics

# Structural characterization of bioactive glasses containing rare earth elements (Gd and/or Yb)

Roger Borges[1], José F. Schneider[2], and Juliana Marchi[1,*]

[1] Centro de Ciências Naturais e Humanas, Universidade Federal do ABC, Avenida dos Estados 5001, Bairro Bangu, Santo André, SP 09210-580, Brazil

[2] Instituto de Física de São Carlos, Universidade de São Paulo, Avenida do Trabalhador São-Carlense 400, Parque Arnold Schmidt, São Carlos, SP, Brazil

**Received:** 17 April 2019
**Accepted:** 21 May 2019
**Published online:** 28 May 2019



## ABSTRACT

Rare earth-containing bioactive glasses are promising materials for biomedical applications like brachytherapy, luminescence-based imaging, magnetic resonance imaging, among others, due to the electronic configuration of rare earth. Although studies of such glasses have continuously been increasing, they still have been poorly studied as biomaterials. In this work, we studied the influence of gadolinium and ytterbium on the structure of bioactive glasses and iron-based bioactive glasses. The glasses were obtained by melt quenching, and their structures were characterized by X-ray diffraction, nuclear magnetic resonance, X-ray photoelectron spectroscopy, electron paramagnetic resonance and scanning electron microscopy. The results showed that the addition of rare earth elements in the glass structure creates more non-bridging oxygen bonds in the silicate network, to satisfy the condition of octahedral coordination of the rare earth ions. An observed $Q^3 \rightarrow Q^2 + Q^1$ depolymerization of the glass network is a factor that could favor bioactivity. In conclusion, our experimental data address the bioactive behavior of rare earth-containing glasses to an increased concentration of non-bridging oxygen bonds and a more fragmented network.

## Introduction

Bioactive glasses (BGs) are amorphous ceramic materials that show biocompatibility when used as biomaterials to repair, to substitute or to treat damaged or unhealthy tissues [1]. These glasses have been used in different biomedical applications, such as bone regeneration, cancer treatment, dentine hypersensitivity, regeneration of soft tissue and drug delivery [2–5].

Rare earth (RE) are interesting elements commonly used as doping species to bring optical and nuclear properties to bioactive glasses, although there are only a few works available in the literature reporting rare earth-containing bioactive glasses, which usually are related to nuclear magnetic resonance imaging, luminescence or brachytherapy applications [6–15].

Address correspondence to E-mail: juliana.marchi@ufabc.edu.br



https://doi.org/10.1007/s10853-019-03715-1

As a consequence, the role of RE in the bioactive glass structure is not completely clear so far.

More recently, Nicollini et al. [16] have proposed Ce-containing bioactive glasses for antioxidant applications because of catalase mimetic effect of cerium, which decompose hydrogen peroxide and prevent cellular stress caused by reactive oxygen species (ROS). It has been proposed that cerium may play different roles in the glass structure depending on the glass composition [16]. In phosphorus-containing glasses, non-bridging oxygens (NBO) of phosphate groups coordinate cerium, whereas in phosphorous-free glasses cerium is coordinated by NBO from silicate species [16, 17]. This behavior suggests that RE elements are coordinated in preferential sites in the glass structure, depending on the glass composition. Furthermore, addition of $CeO_2$ up to 1.5 wt% do not change bioactivity and dissolution, in contrast to glasses containing higher quantities of cerium oxide, which show loss of bioactivity and decrease in solubility that, in turn, are related to a stronger covalent character of Ce–O bond [17].

Molecular dynamics studies have also shown the increase in bond strength of RE–O bonds using theoretical approaches [18–20], giving structural information about yttrium-based BG, and explained the role of yttrium in the glass structure. First, yttrium acts as a modifier ion in the glass network, forming Si–O—Y—O–Si bonds, also as known as yttrium-mediated cross-linked silicate bonds, which have stronger bond energy when compared to other non-bridging oxygen bonds. Second, yttrium tends to decrease the network connectivity by forming yttrium-mediated cross-linked silicate bonds, as new non-bridging oxygen bonds are created. At first glance, it seems reasonable to expect that a decrease in network connectivity may enhance glass dissolution, but, because of the high bond energy of yttrium-mediated cross-linked silicate bonds, the glass dissolution could be almost invariant.

However, following our recent study [21], a small addition of RE ions (2.5 up to 5.0 wt% of gadolinium or ytterbium oxides) in the glass structure promoted bioactivity through fastening calcium and phosphate ions precipitation on the glass surface. On the other hand, such bioactivity was intriguingly contrasted with a delayed dissolution behavior of RE-containing glasses. Considering that bioactivity and dissolution are coupled phenomena in bioactive glasses, we presume that the glass structure has unique information that could help us to elucidate the bioactivity and dissolution behavior observed.

In this work, we studied the glass structure of BG and iron-based bioactive glasses (Fe–BG) doped with rare earth. We choose two different rare earth elements to compare their behavior in the glass structure: ytterbium and gadolinium. The isotope $^{169}Yb$ exhibits suitable properties for brachytherapy (half-life of 32 days and mean gamma ray energy of 93 keV) [22] and works as a sensitizing species in host matrices for luminescence applications [23]. Gadolinium is a proper element as a contrast agent for magnetic resonance imaging due to its paramagnetic properties and relaxation time in the order of nanosecond [24]. BG–Fe were also studied because iron cations on the surface promote interaction with biomolecules related to cell adhesion when the glass is implanted in host tissue and enhances the glass biocompatibility [25]. All the compositions are promised materials for biomedical applications [21, 26]. Finally, this study aims to understand how rare earth ions are changing the glass network of such glasses and then to give further explanations about biological in vitro results already observed.

## Materials and methods

### Glass synthesis

The glass powder of this study were based on the $SiO_2$–$Na_2O$–CaO–$P_2O_5$ system described in [26], using $SiO_2$ (Sigma-Aldrich, 99%), NaOH (Sigma-Aldrich, 99%), CaO (Casa Americana, 99%, Brazil) and $P_2O_5$ (Vetec, 99%, Brazil) as raw materials. The final compositions were defined after incorporation of $Fe_2O_3$ (Sigma-Aldrich, 99%), $Gd_2O_3$ (Sigma-Aldrich, 99.9%) and/or $Yb_2O_3$ (Sigma-Aldrich, 99.9%) into the base BG composition, as shown in Table 1. The powders were mixed in a mortar, placed in a platinum crucible, molten at 1600 °C/2 h (Fortelab FE 1700, Brazil) and quenched onto a brass mold. Then, the glasses were ground in a mortar and sieved, and only particles smaller than 75 μm were used for characterizations.

**Table 1** Glass samples compositions evaluated in this study

| | $SiO_2$ | $Na_2O$ | CaO | $P_2O_5$ | $Fe_2O_3$ | $Gd_2O_3$ | $Yb_2O_3$ |
|---|---|---|---|---|---|---|---|
| BG | 47.28 | 31.39 | 15.33 | 6.00 | – | – | – |
| BG–Fe | 47.03 | 31.22 | 15.25 | 6.00 | 0.50 | – | – |
| BG–Gd | 46.02 | 30.56 | 14.92 | 6.00 | – | 2.50 | – |
| BG–Yb | 46.02 | 30.56 | 14.92 | 6.00 | – | – | 2.50 |
| BG–FeGd | 45.77 | 30.39 | 14.84 | 6.00 | 0.50 | 2.50 | |
| BG–FeYb | 45.77 | 30.39 | 14.84 | 6.00 | 0.50 | | 2.50 |
| BG–FeGdYb | 44.61 | 25.22 | 18.67 | 6.00 | 0.50 | 2.50 | 2.50 |

All values are expressed in weight percentage

## Structural characterization

### *X-ray diffraction*

Diffraction patterns were collected using a D8 Focus diffractometer (Bruker AXS, WI, USA). Glass powders were placed onto the sample holder. The data were collected in a range of $5° < 2\theta < 70°$, at a step time of 10 s and step size of 0.02°, and using Cu Kα radiation.

### *High-resolution nuclear magnetic resonance*

High-resolution nuclear magnetic resonance (NMR) experiments were performed at a magnetic field of 9.4 T in a Varian Unity INOVA spectrometer. In $^{29}$Si-NMR single-pulse experiments, powdered samples were spun at 5 kHz at the magic angle condition in 7 mm zirconia rotors. The $p/2$-pulse duration was 5.0 μs. The recycle delay was optimized for each sample to ensure full relaxation of the magnetization, being 120 s for the BG sample and less than 10 s for glasses with paramagnetic ions (Fe or RE). The number of scans to get a reasonable signal-to-noise ratio varied from 200 for BG to 20000 for BG–FeGd. A sample of kaolinite was used as a secondary standard for the $^{29}$Si chemical shift, with resonance at − 91.5 ppm relative to tetramethylsilane. In $^{31}$P-NMR single-pulse experiments, powdered samples were spun at 9 kHz at the magic angle condition in 4 mm silicon nitride rotors. The $p/2$-pulse duration was 2.5 μs. The recycle delay for full relaxation of the magnetization varied from 120 s for the BG sample to 30 s for BG–Yb and less than 5 s for the rest of the powders. The number of scans to get a reasonable signal-to-noise ratio varied from 380 for BG to 800 for BG–Gd. A liquid sample of 85% $H_3PO_4$ was used as a standard for the $^{31}$P chemical shift.

### *X-ray photoelectron spectroscopy*

XPS characterized the chemical environments of glasses collected in a Thermo Scientific™ K-Alpha™ spectrometer. Both survey and high-resolution scans were collected. For high-resolution analysis Os1 spectrum was analyzed. The analysis was performed in the CASA XPS software (Casa Software Ltd). Peak position was calibrated through normalization of the C1*s* peak at 284.6 eV. A deconvolution approach was used in the O1*s* high-resolution spectrum. For the deconvolution, it was used a Gaussian–Lorentzian line shape, the FWHM was equal for all the three oxygen species analyzed, and the distance between the peaks of each species was fixed as at least 1 eV as already reported in the literature [27].

### *Electronic paramagnetic resonance spectroscopy*

Room temperature electronic paramagnetic resonance (EPR) absorption spectra were collected in a Bruker (Spin EMX 10-2,7 Plus, USA) spectrometer operating at 9.48 GHz with 100 kHz magnetic field modulation.

### *Scanning electron microscopy*

The specimens were prepared by making disks of glass powders dispersed in bakelite. The disks were polished in an automated EcoMet 250 Base Grinder Polisher (Bueler, USA) using a colloidal silica solution, 6 μm and 3 μm diamond colloidal solution. After that, the disks were sputtered with carbon (Leica SCE 200) and then analyzed using an XL-30 Phillips scanning electron microscope equipped with energy-dispersive spectroscopy (EDS) detector. The micrographs were obtained using a backscattered electrons detector to induce a contrast between

regions of different chemical compositions, and EDS spectra were collected at 30 kV.

## Results

An initial characterization using X-ray diffraction was carried out to verify whether the addition of rare earth elements and iron induces any devitrification process during cooling of the powders. The XRD results (Fig. 1) show patterns typical of non-crystalline solids, characterized by the absence of diffraction peaks related to Bragg planes and a broad peak at 32° associated with short-range order of silica tetrahedron.

The $^{29}$Si-NMR spectra of all studied glasses are presented in Fig. 2a. The overlapped resonances of $Q^n$ species are observed, which can be separated through the least-square fitting of Gaussian functions, in order to quantify the respective populations for each site. The central NMR band and the two first-order sidebands were considered in the fitting process. Results from this process are shown in Fig. 2b for powders BG and BG–Yb, where the dashed lines represent the spectral contribution of $Q^1$, $Q^2$ and $Q^3$ species. For the BG glass, the distribution of population resulted in 4% $Q^1$, 33% $Q^2$, 63% $Q^3$. Predominantly, all the glasses show mainly $Q^2$ and $Q^3$ species and a small fraction of $Q^1$, which are following previous NMR studies of glasses with similar compositions [28, 34]. In the $^{29}$Si-NMR spectra of glasses containing Fe or RE, there are two noticeable signatures from the paramagnetism of these species: the broadening of the resonances and the increase in the intensity of the spinning sidebands. These effects are particularly strong in glasses with a high concentration of paramagnetic ions, as BG–Fe–Yb, or those containing Gd, the species with the highest magnetic moment. In BG–Fe and BG–Yb glasses, these effects are moderate, allowing the analysis of the $Q^n$ distribution. The spectrum from the BG–Yb glass show more broadened resonances with a silicon distribution of 9% $Q^1$, 36% $Q^2$, 54% $Q^3$, 1% $Q^4$, indicating the increase in $Q^2$ to the expense of $Q^3$ species when compared to the BG or BG–Fe glasses. This difference of silicon speciation can be expressed in terms of the average connectivity of the silicate network, NC = 2 BO/NBO.

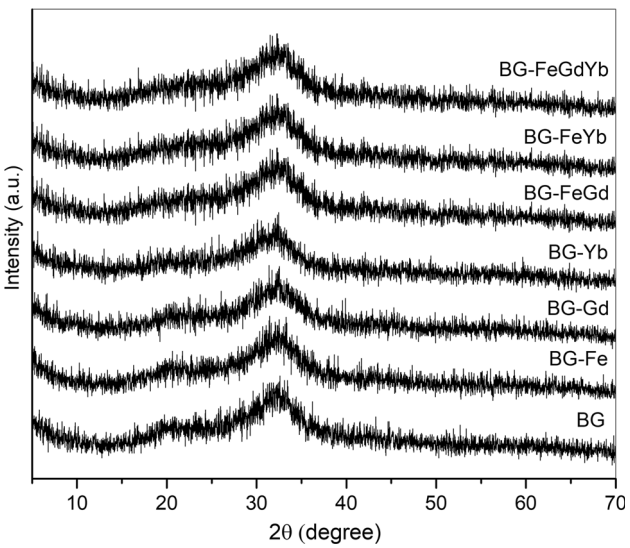


**Figure 1** XRD diffraction patterns of glass samples. The absence of diffraction peaks indicates that glassy nature of the materials.

The experimental NC calculated using the $Q^n$ populations determined by $^{29}$Si-NMR in BG and BG–Fe glasses was 1.83, while for the BG–Yb glass it was 1.61, revealing that the rare earth-containing glasses possess a less connected silicate network. For the other glasses, precise quantification of silicon species and calculation of NC were not possible due to the loss of resolution associated with the stronger paramagnetic effects. Then, we used O1*s* high-resolution XPS to calculate NC for the other glasses. In Fig. 3a, a typical deconvolution approach for O1*s* high-resolution spectra is presented for the BG–Yb glass. The NC derived from XPS was calculated for all the glasses (Fig. 3b), and the values obtained for BG, BG–Fe and BG–Yb were compared with those results from $^{29}$Si-NMR to check the reliability of XPS-derived NC, as given in Table 2. The differences of NC values from XPS and $^{29}$Si-NMR for BG, BG–Fe and BG–Yb were less than 4% and showed the same trend with glass composition, supporting the reliability of the quantifications.

The $^{31}$P-NMR spectra of the glasses (Fig. 2c) show the main resonance between 11 and 9 ppm. This peak is related to the orthophosphate environment of phosphorous ($Q^0$) associated with Na, indicating that phosphate groups play a role as modifiers anions rather than network formers. There is also a shoulder in the $^{31}$P-NMR, clearly resolved in the spectra of BG and BG–Fe, which can be attributed to $Q^0$ associated with Ca. The paramagnetic broadening of the $^{31}$P resonances reveals the proximity of RE ions to phosphorous. As in the case of $^{29}$Si-NMR, the most intense effects are caused by Gd. There are no

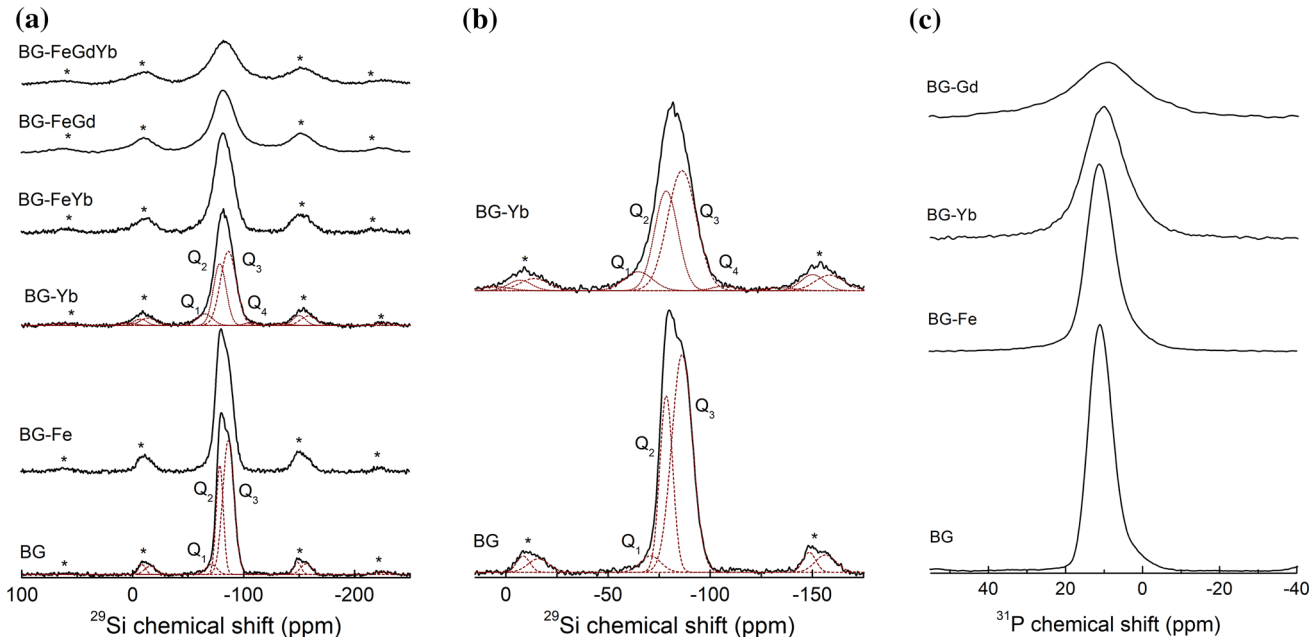


**Figure 2** High-resolution NMR spectra of the glasses: **a** $^{29}$Si-NMR; **b** Gaussian least-square fitting of $^{29}$Si-NMR for BG and BG–Yb glasses; **c** $^{31}$P-NMR spectra. Asterisks: spinning sidebands.

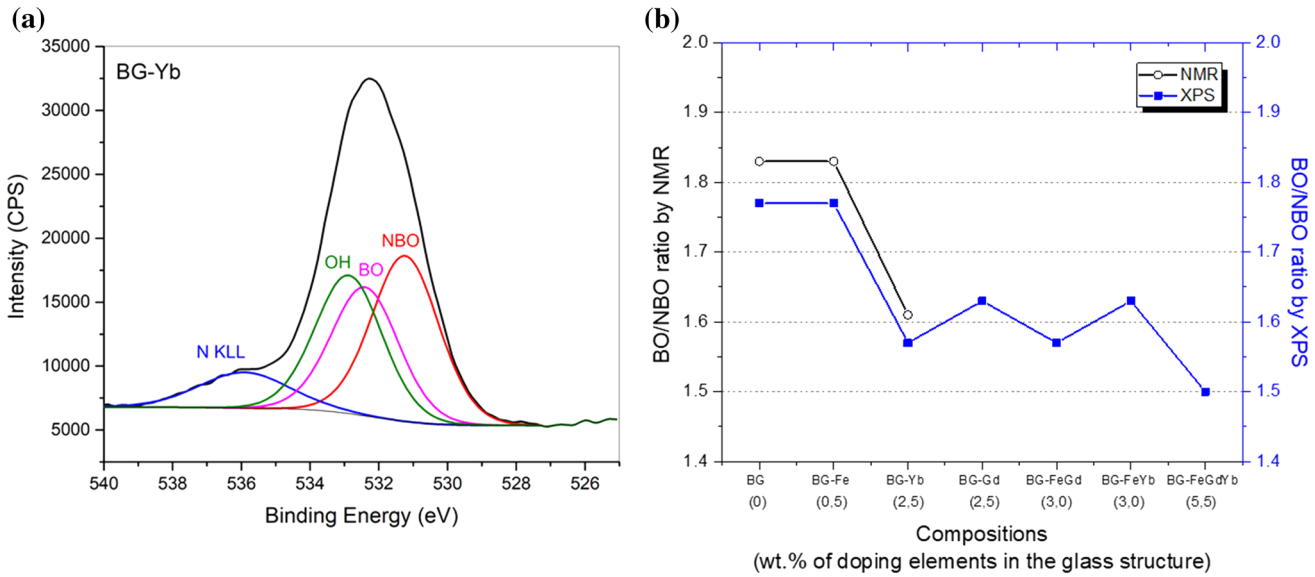


**Figure 3** O1*s* high-resolution XPS results: **a** sample of a deconvoluted O1*s* high-resolution spectrum; **b** network connectivity BO/NBO ratios obtained from NMR (black circles) and XPS (blue squares).

indications of new phosphorous sites in Fe- or RE-doped glasses.

Regarding EPR results, as the Fe and Gd signals overlap, the results were divided into Gd-containing and Gd-free glasses, which are presented in Fig. 4a, b, respectively. Concerning the EPR spectra of Gd-containing glasses (Fig. 4a), it was noted the typical U-spectrum, which contains symmetric lines at $\approx$ 1200, 2400 and 3580 G that stands for $g \approx 5.8$, 2.8 and 2.0, respectively, and are characteristic for $Gd^{3+}$ species [29, 30]. An asymmetric line at 1640 G ($g \approx 4.12$) is also assigned as $Gd^{3+}$ sites in glasses [29].

Figure 4b shows the EPR spectra of Gd-free glasses in which $Fe^{3+}$ lines can be observed. The main lines from the EPR spectra are characterized by $g \approx 4.24$

**Table 2** Quantification of BO and NBO species obtained through $^{29}$Si-NMR and O1*s* high-resolution XPS

| | Experimental (NMR) | | Experimental (XPS) | |
|---|---|---|---|---|
| | BO (%) | NBO (%) | BO (%) | NBO (%) |
| BG | 48 | 52 | 47 | 53 |
| BG–Fe | 48 | 52 | 47 | 53 |
| BG–Yb | 45 | 55 | 44 | 56 |
| BG–Gd | – | – | 45 | 55 |
| BG–FeYb | – | – | 45 | 55 |
| BG–FeGd | – | – | 44 | 56 |
| BG–FeGdYb | – | – | 43 | 57 |

and 2.0 resonance lines [31, 32]. The line at $g \approx 4.24$ is assigned to isolated $Fe^{3+}$ ions placed in sites of low symmetry and high crystal fields, while that at $g \approx 2.0$ is assigned to $Fe^{3+}$ ions placed in sites of octahedral symmetry and low crystal field, or even associated with ions clusters. Another minor EPR signal is also observed at $g \approx 7.60$ which is related to $Fe^{3+}$ ions disposed of in sites of axial symmetry [31].

The results from SEM–EDS analysis (Fig. 5), reveal that iron remains segregated in the glass matrix. For this analysis, only samples containing RE were chosen, once the focus was to evaluate the influence of RE on iron species, and the results presented here are from BG–FeGd glass. This segregation was noted by the EDS spectra, which shows the presence of all the glass elements in the spectrum in Fig. 5b (related to point 1 in Fig. 5a), and shows only the presence of Fe and O in the spectrum in Fig. 5c (related to point 2 in Fig. 5a).

## Discussion

The XRD results evidenced the glassy nature of the powders and showed that the additions of Gd, Yb, and Fe do not induce any glass devitrification. It was only observed that part of the iron oxide remains

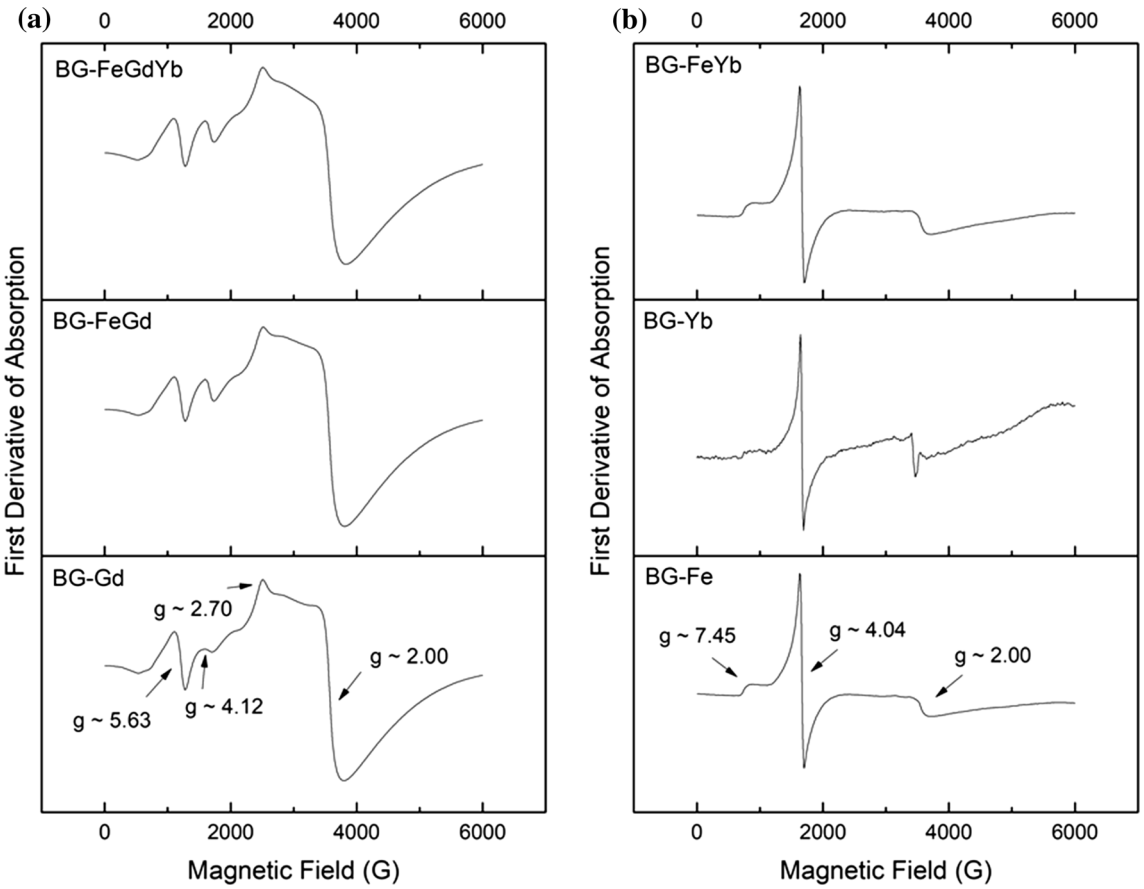


**Figure 4** EPR results of studied glasses: **a** EPR spectra of Gd-containing glasses; **b** EPR spectra of Gd-free glasses.

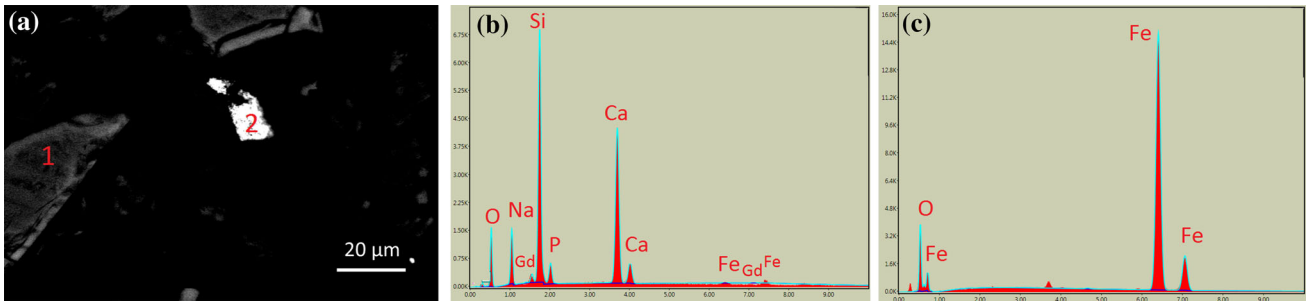


**Figure 5** Microstructural analysis of BG–FeGd compositions: **a** typical SEM micrograph **b**–**c** EDS analysis of the two different particles from SEM micrograph, points 1 and 2, respectively. Similar results were observed in all the iron-containing compositions.

segregated in the glass structure, as noted in the SEM–EDS analysis. Taken those facts into account, we assumed that the addition of RE caused the effects observed in the network connectivity (NC).

The NC values obtained by $^{29}$Si-NMR and O1*s* XPS suggest that RE-containing glasses have a less connected network than the pristine glass. The $^{29}$Si-NMR for the BG–Yb glass suggests the occurrence of glass depolymerization associated with $Q^3 \rightarrow Q^2 + Q^1$ conversion, which is associated with an increase in NBO bonds concentration. If we consider that the decrease in NC observed in the O1*s* XPS spectra for glasses containing RE occurred by a mechanism similar to that of BG–Yb glass, we could infer that the decrease in NC of these glasses is also related to an increase of $Q^2$ and $Q^1$ species at the expense of $Q^3$.

The EPR results can explain the formation of new NBO species. The different *g*-values have different meanings and interpretations for the glass structure. In Gd-containing glasses, the broad line around $g \approx 2$ is attributed to magnetic clusters of $Gd^{3+}$ or Gd–O–Gd bonds where gadolinium ions interact with each other by superexchange interactions. Values of $g \approx 6.0$ and 2.8 are related to $Gd^{3+}$ in tetrahedral, octahedral or cubic sites of weak crystal field and coordination number higher than six, which leads many researchers to assign these *g*-values as $Gd^{3+}$ ions playing a glass modifier role, i.e., coordinated by non-bridging oxygens. The $g \approx 4.8$ is characteristic of $Gd^{3+}$ ions in sites of strong crystal fields, having a low coordination number, and it is assigned to gadolinium ions playing a glass former role. The fact that the most intense line is that of $g \approx 2$ means that most of the gadolinium ions are clustered in the glass structure, while the other part plays an intermediated role. Probably, $Yb^{3+}$ may behave similarly; however, it was not possible to carry out experiments at low temperature in which $Yb^{3+}$ lines can be observed in the EPR spectrum. These results can be contrasted with previous studies of Ce-containing BGs [16, 17]. In Ce–BG, cerium acts as a glass former when in the presence of phosphate groups and as a glass modifier when present in a silicate environment. Once we observed an intermediate role of $Gd^{3+}$ and $Yb^{3+}$ ions in the glass structure, one can infer that the RE are found in both silicate and phosphate environments, if assumed that $Gd^{3+}$ and $Yb^{3+}$ behave like $Ce^{3+}$ in the glass structure. This hypothesis is consistent with the XPS and $^{31}$P-NMR results because it was noted a decrease in glass connectivity when RE were added in the glass structure. Moreover, it was also observed a broadening of phosphorus resonances in the $^{31}$P-NMR results, suggesting that RE were close to both silicate and phosphate species.

Taken into account the $^{29}$Si-NMR and the EPR results, it is acceptable to assume that the modifier role of RE is leading to the $Q^3 \rightarrow Q^2 + Q^1$ conversion. In other works from the literature, the addition of glass modifiers in bioactive glasses has been related to such silicon species transformation [33] and to the addition of RE elements in aluminosilicate glasses [34, 35]. Particularly in aluminosilicate glasses, Iftekhar et al. [34] associated the increase in $Q^2$ silicon species with the octahedral coordination of rare earth elements. Then, considering that rare earth elements are replacing Ca and Na in the glass structure and have octahedral coordination as observed in the EPR results, it is expected that $^{29}$Si-NMR present a higher fraction of $Q^2$ species.

Regarding the Gd-free compositions, where $Fe^{3+}$ lines are observed in EPR, the EPR spectra do not change as RE are added in the glass structure. This result suggests that the rare earth does not change the

iron coordination, which may be somewhat influenced by iron solubility in the glass structure, as already observed in the SEM–EDS results (Fig. 5). In fact, in Gd-free glasses, while signals at $g \approx 4.24$ and 7.60 are related to iron species dispersed in the glass structure, the less intense line at $g \approx 2.0$ shows that a minor, but significant, fraction of iron was not dissolved in the glass structure. This result is also consistent with the systematic observation of weak paramagnetic effects in the $^{29}$Si and $^{31}$P $^{23}$ NMR spectra of the BG–Fe sample. The $^{29}$Si-NMR spectra even showed identical silicon speciation in BG and BG–Fe glasses, which suggest that even though some quantities of iron oxide were added in the glass structure, there is no fundamental difference in the structure of the silicate networks because the number of irons not segregated was not enough to lead to significant changes.

These changes in glass network connectivity may display an influence on bioactivity, and special attention must be given to the bond strength of Si–O–RE–O–Si, also as known as RE-mediated cross-linking silicon tetrahedral. If breaking these bonds is less energetically favorable than breaking non-RE-mediated cross-linking silicon tetrahedral, a decrease in the dissolution kinetics is expected [18]. In fact, in our previous work [21] we experimentally showed that RE-containing glasses (RE = Gd and Yb) dissolve slower than BG due to the higher bond strength of RE-mediated cross-linking silicon tetrahedrons. In the same work, we also showed that bioactivity starts earlier in RE-containing glasses than in BG. Considering the depolymerization phenomena observed in this work, one can infer that the earlier bioactivity in RE-containing glasses might be addressed to more fragmented network connectivity, which favors the release of calcium and phosphate ions.

The results of $^{31}$P-NMR give new perspectives about the bioactivity of these glasses. The environments of phosphorus and calcium are crucial along the bioactivity reactions because their dissolution is responsible for locally saturating the body fluid and then precipitating calcium phosphate onto the glass surface. Hill and Brauer [36] pointed out that the dissolution of the silicate and the phosphate phases happens as separate phenomena. Thus, the fact that RE and Fe did not change the phosphorus speciation, i.e., only $Q^0$ groups, meaning that the dissolution of the orthophosphate phases may not be affected as well.

## Conclusions

Bioactive glasses doped with rare earth elements (RE = Gd and/or Yb) and iron were successfully obtained. Rare earth played an intermediate role in the glass structure, i.e., acting as glass formers and modifiers. The structural characterization suggested a $Q^3 \rightarrow Q^2 + Q^1$ conversion when RE were added in the glass structure, which leads to the creation of new non-bridging oxygens favored by octahedral coordination of RE. This decrease in network connectivity might be the phenomenon responsible for counterbalancing the strong covalent character of Si–O–RE bonds when these glasses are immersed in fluids. When iron was added in the glass composition, it leads to phase separation, which means that iron oxide remains partially segregated in the glass structure. This work encourages further experimental development of RE-containing bioactive glasses aiming at different biomedical applications.

## Acknowledgements

The authors gratefully acknowledge Profa. Dra. Marcia Spinace and her graduate student MSc. Asaph for their support on the FTIR analysis, and Prof. Dr. Carlos Rettori and Dr. Michael Cabrera-Baez for their support on the EPR measurements and analysis. We are grateful to the Centro em Ciência e Tecnologia dos Materiais at IPEN/CNEN São Paulo, Brazil, for their support on the scanning electron microscopy, and to Central Experimental Multiusuário CEM/UFABC, Brazil, for the facilities support. The authors also appreciate the financial support provided by UFABC and Brazilian Founding Agencies such as FAPESP (2014/19308-8, 2013/07793-6, 2016/16512-0 and 2011/19924-2) and CNPq (308142/2015-2, 130637/2016-5, 402066/2016-2 and 08142/2015-2).

## Compliance with ethical standards

**Conflict of interest** The authors do not have any conflict of interest.

## References

[1] Marchi J (2016) Biocompatible glasses: from bone regeneration to cancer treatment, 1st edn. Springer International

Publishing, Cham. https://doi.org/10.1007/978-3-319-44249-5

[2] Lopez TCC, Diniz IMA, Ferreira LS, Marchi J, Borges R, de Cara SPHM, D'Almeida-Couto R, Marques MM (2017) Bioactive glass plus laser phototherapy as promise candidates for dentine hypersensitivity treatment. J Biomed Mater Res Part B Appl Biomater 105:107–116. https://doi.org/10.1002/jbm.b.33532

[3] Borges R, Kai KC, Marchi J (2016) Biocompatible glasses for controlled release technology. In: Marchi J (ed) Biocompatible glasses—from bone regeneration to cancer treatment, 1st edn. Springer International, Cham, pp 285–315. https://doi.org/10.1007/978-3-319-44249-5

[4] Aspasio RD, Borges R, Marchi J (2016) Biocompatible Glasses for cancer treatment. In: Marchi J (ed) Biocompatible glasses—from bone regeneration to cancer treatment, 1st edn. Springer International, Cham, pp 249–265. https://doi.org/10.1007/978-3-319-44249-5

[5] Mokhtari S, Skelly KD, Krull EA, Coughlan A, Mellott NP, Gong Y, Borges R, Wren AW (2017) Copper-containing glass polyalkenoate cements based on $SiO_2$–ZnO–CaO–SrO–$P_2O_5$ glasses: glass characterization, physical and antibacterial properties. J Mater Sci 52:8886–8903. https://doi.org/10.1007/s10853-017-0945-5

[6] Sadeghi M, Taghdiri F, Hosseini SH, Tenreiro C, Tenreiro C (2010) Monte Carlo calculated TG-60 dosimetry parameters for the $\beta^-$ emitter $^{153}$Sm brachytherapy source. Med Phys 5370:5369–5395. https://doi.org/10.1118/1.3488971

[7] Hosseini SH, Enferadi M, Sadeghi M (2013) Dosimetric aspects of Ho brachytherapy biodegradable glass seed. Appl Radiat Isot 73:109–115. https://doi.org/10.1016/j.apradiso.2012.12.002

[8] Roberto WS, Pereira MM, Campos TPR (2003) Dosimetric analysis and characterization of radioactive seeds produced by the sol-gel method 242:579–582. https://doi.org/10.4028/www.scientific.net/KEM.240-242.579

[9] Campos TPR, Andrade JPL, Costa IT, Silva CHT (2008) Study of the Sm-153 seeds degradation and evaluation of the absorbed dose in rabbit's liver implants. Prog Nucl Energy 50:757–766. https://doi.org/10.1016/j.pnucene.2008.01.007

[10] El-Kady AM, Ali AF, Rizk RA, Ahmed MM (2012) Synthesis, characterization and microbiological response of silver doped bioactive glass nanoparticles. Ceram Int 38:177–188. https://doi.org/10.1016/j.ceramint.2011.05.158

[11] Taghdiri F, Sadeghi M, Hosseini SH, Athari M (2011) TG-60 dosimetry parameters calculation for the $\beta^-$ emitter $^{153}$Sm brachytherapy source using MCNP, Iran. J Radiat Res 9:103–108

[12] Khorshidi A, Ahmadinejad M, Hosseini SH, N-particle C (2015) Evaluation of a proposed biodegradable $^{188}$Re source for brachytherapy application: a review of dosimetric parameters. Medicine (Baltimore) 94:1–7. https://doi.org/10.1097/MD.0000000000001098

[13] Roberto WS, Pereira MM, Campos TPR (2003) Structure and dosimetric analysis of biodegradable glasses for prostate cancer treatment. Artif Organs 27:432–436

[14] Fan Y, Yang P, Huang S, Jiang J, Lian H, Lin J (2009) Luminescent and mesoporous europium-doped bioactive glasses (MBG) as a drug carrier. J Phys Chem C 113:7826–7830. https://doi.org/10.1021/jp900515x

[15] Huang S, Kang X, Cheng Z, Ma P, Jia Y, Lin J (2012) Electrospinning preparation and drug delivery properties of $Eu^{3+}$/$Tb^{3+}$ doped mesoporous bioactive glass nanofibers. J Colloid Interface Sci 387:285–291. https://doi.org/10.1016/j.jcis.2012.08.004

[16] Nicolini V, Varini E, Malavasi G, Menabue L, Menziani MC, Lusvardi G, Pedone A, Benedetti F, Luches P (2016) The effect of composition on structural, thermal, redox and bioactive properties of Ce-containing glasses. Mater Des 97:73–85. https://doi.org/10.1016/j.matdes.2016.02.056

[17] Leonelli C, Lusvardi G, Malavasi G, Menabue L, Tonelli M (2003) Synthesis and characterization of cerium-doped glasses and in vitro evaluation of bioactivity. J Non Cryst Solids 316:198–216. https://doi.org/10.1016/S0022-3093(02)01628-9

[18] Christie JK, Malik J, Tilocca A (2011) Bioactive glasses as potential radioisotope vectors for in situ cancer therapy: investigating the structural effects of yttrium. Phys Chem Chem Phys 13:17749–17755. https://doi.org/10.1039/c1cp21764j

[19] Christie JK, Tilocca A (2012) Integrating biological activity into radioisotope vectors: molecular dynamics models of yttrium-doped bioactive glasses. J Mater Chem 22:12023–12031. https://doi.org/10.1039/c2jm31561k

[20] Tilocca A (2015) Realistic models of bioactive glass radioisotope vectors in practical conditions: structural effects of ion exchange. J Phys Chem C 119:17442–27448. https://doi.org/10.1021/acs.jpcc.5b07804

[21] Zambanini T, Borges R, Delfino GP, Sousa IP, Marques MM, Marchi J (2018) Dissolution, bioactivity behavior and cytotoxicity of rare earth-containing bioactive glasses (RE = Gd, Yb). Int J Appl Ceram Technol. **(Accepted for publication)**

[22] Loft SM, Coles IP, Dale RG (1992) The potential of ytterbium 169 in brachytherapy: a brief physical and radiobiological assessment. Br J Radiol 65:252–257. https://doi.org/10.1259/0007-1285-65-771-252

[23] Cornejo CR (2016) Luminescence in rare earth ion-doped oxide compounds. In Thirumalai J (Ed) Luminescence—an

outlook on the phenomena and their applications, 1st edn. IntechOpen, London. https://doi.org/10.5772/65185

[24] Hu F, Wei X, Qin Y, Jiang S, Li X, Zhou S, Chen Y, Duan C-K, Yin M (2016) $Yb^{3+}/Tb^{3+}$ co-doped $GdPO_4$ transparent magnetic glass–ceramics for spectral conversion. J Alloys Compd 674:162–167. https://doi.org/10.1016/j.jallcom.2016.03.040

[25] Cannas M, Indemini E, Krajewski A, Ravaglioli A, Contoli S (1990) In vitro observations of iron-doped bioactive glasses. Biomaterials 1:281–285

[26] Borges R, da Silva AC, Marchi J (2012) Evaluation of the bioactivity behavior of a 48 wt% $SiO_2$ bioglass through experiments in simulated body fluid. Mater Sci Forum 727–728:1238–1242. https://doi.org/10.4028/www.scientific.net/MSF.727-728.1238

[27] Nesbitt HW, Bancroft GM, Henderson GS, Ho R, Dalby KN, Huang Y, Yan Z (2010) Bridging, non-bridging and free ($O^{2-}$) oxygen in $Na_2O$–$SiO_2$ glasses: an X-ray photoelectron spectroscopic (XPS) and nuclear magnetic resonance (NMR) study. J Non Cryst Solids 357:170–180. https://doi.org/10.1016/j.jnoncrysol.2010.09.031

[28] Lockyer MWG, Holland D, Dupree R (1995) NMR investigation of the structure of some bioactive and related glasses. J Non Cryst Solids 188:207–219. https://doi.org/10.1016/0022-3093(95)00188-3

[29] Rada S, Dan V, Rada M, Culea E (2010) Gadolinium-environment in borate–tellurate glass ceramics studied by FTIR and EPR spectroscopy. J Non Cryst Solids 356:474–479. https://doi.org/10.1016/j.jnoncrysol.2009.12.011

[30] Malchukova E, Boizot B, Ghaleb D, Petite G (2006) β-Irradiation effects in Gd-doped borosilicate glasses studied by EPR and Raman spectroscopies. J Non Cryst Solids 352:297–303. https://doi.org/10.1016/j.jnoncrysol.2005.11.003

[31] Eniu D, Gruian C, Vanea E, Patcas L, Simon V (2015) FTIR and EPR spectroscopic investigation of calcium-silicate glasses with iron and dysprosium. J Mol Struct 1084:23–27. https://doi.org/10.1016/j.molstruc.2014.12.020

[32] Shankhwar N, Kothiyal GP, Srinivasan A (2014) Understanding the magnetic behavior of heat treated CaO–$P_2O_5$–$Na_2O$–$Fe_2O_3$–$SiO_2$ bioactive glass using electron paramagnetic resonance studies. Phys B Condens Matter 448:132–135. https://doi.org/10.1016/j.physb.2014.03.070

[33] Pedone A, Charpentier T, Malavasi G, Menziani MC (2010) New insights into the atomic structure of 45S5 bioglass by means of solid-state NMR spectroscopy and accurate first-principles simulations. Chem Mater 22:5644–5652. https://doi.org/10.1021/cm102089c

[34] Iftekhar S, Pahari B, Okhotnikov K, Jaworski A, Stevensson B, Grins J, Edén M (2012) Properties and structures of $RE_2O_3$–$Al_2O_3$–$SiO_2$ (RE = Y, Lu) glasses probed by molecular dynamics simulations and solid-state NMR: the roles of aluminium and rare-earth ions for dictating the microhardness. J Phys Chem C 116:18394–18406. https://doi.org/10.1021/jp302672b

[35] Marchi J, Morais DS, Schneider J, Bressiani JC, Bressiani AHA (2005) Characterization of rare earth aluminosilicate glasses. J Non Cryst Solids 351:863–868. https://doi.org/10.1016/j.jnoncrysol.2005.01.078

[36] Hill RG, Brauer DS (2011) Predicting the bioactivity of glasses using the network connectivity or split network models. J Non Cryst Solids 357:3884–3887. https://doi.org/10.1016/j.jnoncrysol.2011.07.025